Tellus (1988), *40A*, 248–255

SHORT CONTRIBUTION

Climatology of polar lows over the Norwegian and Barents Seas

By TORLEIV ESE, INGOLF KANESTRØM and KAARE PEDERSEN, *Institute of Geophysics, University of Oslo, PO Box 1022 Blindern, 0315 Oslo 3, Norway*

(Manuscript received 14 June 1986; in final form 9 September 1987)

ABSTRACT

The large-scale flow pattern during the formation of polar lows over the Norwegian and Barents Seas has been studied. The results indicate that in most cases a strong northerly airflow is located close to the east coast of Greenland. The geographical distribution of polar lows suggests a division of the events into two groups, a western group consisting of the lows first observed west of 5° E, and an eastern group consisting of those first observed east of the same longitude. Mean maps for each group were constructed for the winter season, and they show large anomalies. The strongest negative anomaly in the 500 mb height is found over the Norwegian Sea. The anomaly is −230 gpm for the events west of 5° E, and −179 gpm for those east of 5° E. For polar lows developing in the western sector, the largest positive anomaly, +198 gpm, is associated with the Azores High. When polar lows are formed in the eastern sector, the strongest positive anomaly is associated with the ridge over Greenland; the cold air in the strong northerly flow east of Greenland is then up to 8 °C colder than normal. The location of this cold anomaly gives a westward tilt of the anomaly pattern with height.

1. Introduction

The polar lows observed in the Norwegian and Barents Seas appear during cold air outbreaks mainly in the period November through March. They have earlier been detected through manifestation of strong winds or large pressure tendencies on one or more synoptic stations. In later years, satellite images have given additional possibilities to detect polar lows. Case studies of polar lows, defined in a broad sense, have been presented by several authors, e.g., by Harley (1960), Harrold and Browning (1969), Stevenson (1968), Rabbe (1975), Wilhelmsen (1981) and Hoem et al. (1984). A climatological study of gale producing polar lows near Norway was given by Wilhelmsen (1985), and climatological aspects of polar lows have been studied by Carleton (1985) and Businger (1985). Businger (1985) computed a composite 500 mb map by averaging the 500 mb geopotential heights for the starting days (key days) of all polar low events observed over the Norwegian and Barents Seas. The events were observed during the period September through April. He computed an anomaly map by subtracting the climatological 500 mb geopotential height field for the season October through April (1965–1980) from the composite map.

In this paper, we present similar anomaly maps. However, we have divided the polar low events into 2 geographical groups, and we have studied the events for the winter season December through March only. We have also computed the composite sea-level pressure and the 1000–500 mb thickness fields for the 2 groups.

2. The data and climatology of polar lows

In this study, we used observational data of polar lows, consisting of starting date and location for the period January 1971 through January 1983 provided by Lystad and Wilhelmsen (personal communication). A list of the key days (starting days) of each observed polar low for the period January 1971 through January 1983 is given in Table 1. For the period January 1971–March 1982 only those lows that affected the Norwegian coast were included. After March 1982 also those polar lows not affecting the coast are included in the data. The data are almost the same as those listed by Businger (1985) for the period October 1971–March 1981, although, our data set covers a longer time period. For the winter season (December–March), which is discussed in this paper, we have 22 polar low events in addition to those listed by Businger.

Table 1. *The dates of polar lows that developed a mature state in the period January 1971–January 1983, except 1980 (M. Lystad and K. Wilhelmsen, personal communication)*

Western sector GMT				Eastern sector GMT			
December–March							
00	22	March	1972	00	24	March	1972
00	13	Dec.	1973	00	17	Dec.	1972
00	18	Dec.	1973	12	16	March	1973
12	8	Feb.	1974	00	18	Dec.	1973
00	15	March	1975	00	31	Dec.	1975
00	12	Jan.	1976	00	1	Jan.	1976
00	29	March	1976	00	3	Jan.	1976
12	30	March	1976	12	5	Jan.	1976
00	29	Dec.	1977	00	5	March	1977
00	2	Jan.	1978	12	26	March	1977
12	3	Jan.	1981	00	11	Jan.	1978
12	8	Jan.	1981	00	23	Jan.	1978
12	14	Jan.	1981	00	17	Feb.	1978
00	5	Dec.	1982	12	26	Dec.	1978
00	13	Dec.	1982	00	28	Jan.	1979
12	17	Dec.	1982	12	30	Dec.	1979
12	21	Dec.	1982	00	3	March	1981
12	7	Jan.	1983	00	27	March	1981
12	17	Jan.	1983	12	3	Dec.	1981
				12	26	Jan.	1982
				00	25	Feb.	1982
				12	11	Dec.	1982
				00	13	Dec.	1982
				00	14	Dec.	1982
				00	16	Dec.	1982
				12	12	Jan.	1983

Table 1—*continued*

Western sector GMT				Eastern sector GMT			
April–June							
00	25	April	1973	00	14	April	1973
00	27	April	1973	00	6	April	1975
00	12	April	1975	00	28	May	1975
12	17	April	1977	00	14	April	1979
September–November							
00	10	Nov.	1973	00	12	Oct.	1971
12	16	Nov.	1973	12	25	Sept.	1972
00	23	Nov.	1973	00	12	Sept.	1973
00	5	Sept.	1973	00	8	Oct.	1973
12	17	Nov.	1977	00	11	Nov.	1973
12	18	Nov.	1977	00	23	Nov.	1973
12	12	Oct.	1981	00	17	Oct.	1975
00	3	Nov.	1982	00	17	Nov.	1975
				00	20	Nov.	1975
				00	21	Nov.	1975
				00	26	Sept.	1976
				00	23	Nov.	1976
				12	19	Nov.	1978

We have also used observational data from the National Climate Center (NMC), supplied by the National Center for Atmospheric Research. The upper air data used are daily 500 mb geopotential heights at 00 GMT and 12 GMT. This data set covers the period from 1946 through 1984. The surface data consists of daily sea level pressure (SLP) maps for the period January 1946–January 1983 (with 1980 missing). The data are given in the octogonal NMC-grid. The grid length at 60°N is 381 km.

During the period 17 October 1971 through 17 January 1983, altogether 74 polar lows were identified (Table 1). The distribution as a function of longitude of their position at the time of discovery has two outstanding maxima, one in the Norwegian Sea and the other in the Barents Sea (Fig. 1). It therefore seemed reasonable to divide the events into two groups, a western group consisting of lows first observed west of longitude 5°E, and an eastern group consisting of

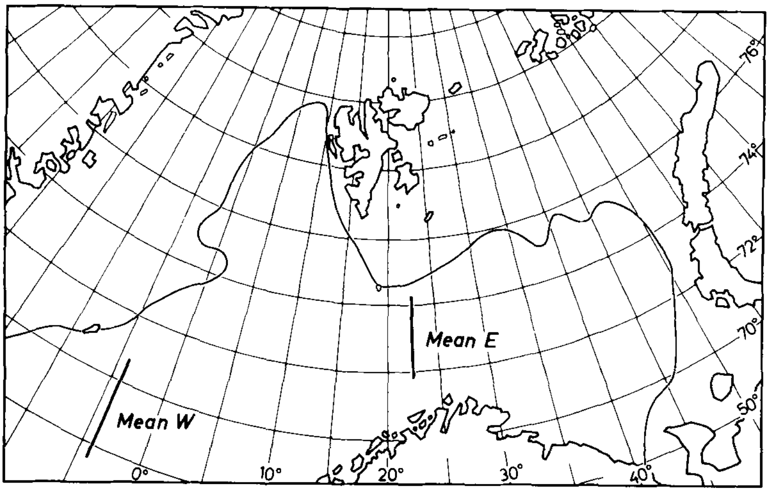

Fig. 1. The average position of the ice edge in February for the years 1971–1980. Mean W and Mean E show the mean value of the longitude for the polar lows in the western and eastern groups.

those first observed east of this longitude. The eastern group consists of 43 polar lows with mean longitude 22.8°E and a standard deviation of 8.7° longitude. The corresponding numbers for the 31 polar lows in the western group are 4.5°W and 7.5°, respectively. The longitudinal mean positions for the two groups are shown in Fig. 1. This figure also shows the average position of the ice edge in February for the years 1971–1980, as given by Vinje (1985). The line of separation between the two groups, the 5°E meridian, is located over the open water west of Spitsbergen.

In order to obtain anomaly maps, Businger computed the 500 mb mean geopotential height field for October through April, 1965–1980. However, the monthly climatological mean sea-level pressure field and the 500 mb mean height field for October, November and especially for April are different from the other winter months. The monthly mean maps for the period December through March are rather similar. We will therefore use seasonal climatological maps for these four winter months.

In the years 1971–1983, we found 19 winter season polar low events in the western sector and 26 events in the eastern sector. The distribution as a function of longitude of these lows at the key day is similar to the distribution found for the total number of polar lows.

For most cases of observed polar lows, we found a strong northerly air flow over the Norwegian Sea or a north-easterly flow over the Barents Sea. The position of the large-scale low pressure centers for the days when polar lows were first observed is given in Fig. 2. The

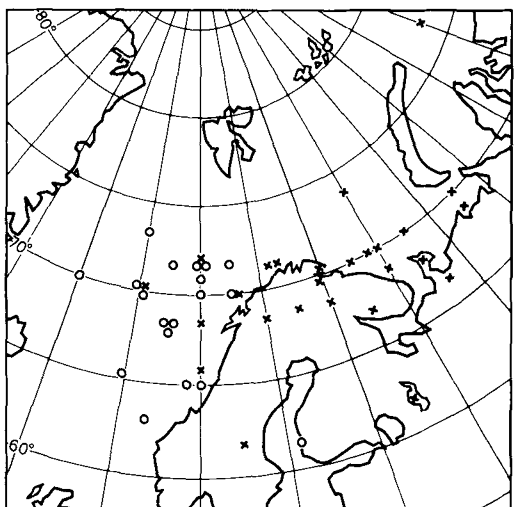

Fig. 2. The positions of the large-scale synoptic low pressure centre for the days when polar lows were observed. The positions of the synoptic-scale low centre when a polar low is observed in the western sector are marked with circles. Crosses are used to indicate the position of synoptic-scale lows when polar lows are observed in the eastern sector.

position is marked by a circle for the western sector and a cross for the eastern sector. For the eastern sector, the large scale low pressure centers are scattered over a large area.

3. Composite pictures of the synoptic maps

Composite and anomaly maps were computed for the key days for each of the two groups defined in Section 2. In the following, we will consider only maps for the winter season (December through March).

3.1. The flow pattern at the sea level

Fig. 3 gives the winter season climatological sea level pressure map (SLP) for the period 1946–1979. The composite SLP map (mean map) for the 19 events that occurred in the western sector is given in Fig. 4a. The climatological SLP map shows a weak trough in the Norwegian Sea (cf. Fig. 3). In the composite SLP map, however, we find a deep low pressure located at 70° N and 5° E with a centre value of 982 mb. Fig. 4b gives the composite SLP map for the 26 eastern sector events. The low pressure centre is at 70° N and 35° E, with a centre value of 990 mb. These two lows in Fig. 4a and 4b will in the following be denoted as the 70° N lows.

Another outstanding feature in the SLP composite maps for the two sectors is found near the Azores High. For the eastern sector events, the Azores High has a position and pressure value equal to the climatological value. For the western sector events, however, the high pressure centre is located at 45° N and 25° W with a centre value

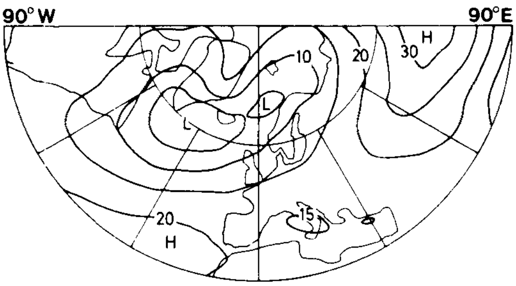

Fig. 3. The climatological surface map (contour intervals 5 mb relative to 1000 mb) for the winter season of the years 1946–1979.

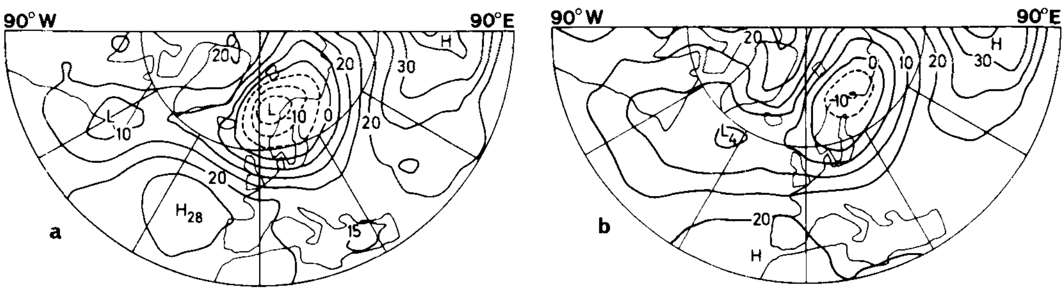

Fig. 4. The composite sea level map (contour interval 5 mb) for the polar low events during the winter season (Table 1). Dashed contours are used for values less than 1000 mb; (a) western sector, (b) eastern sector.

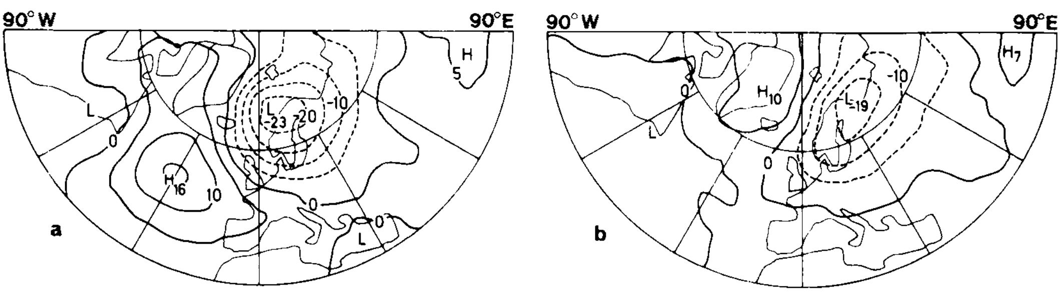

Fig. 5. The sea level anomaly field (contour interval 5 mb) for the polar low events during the winter season. Dashed contours are used for negative values; (a) western sector, (b) eastern sector.

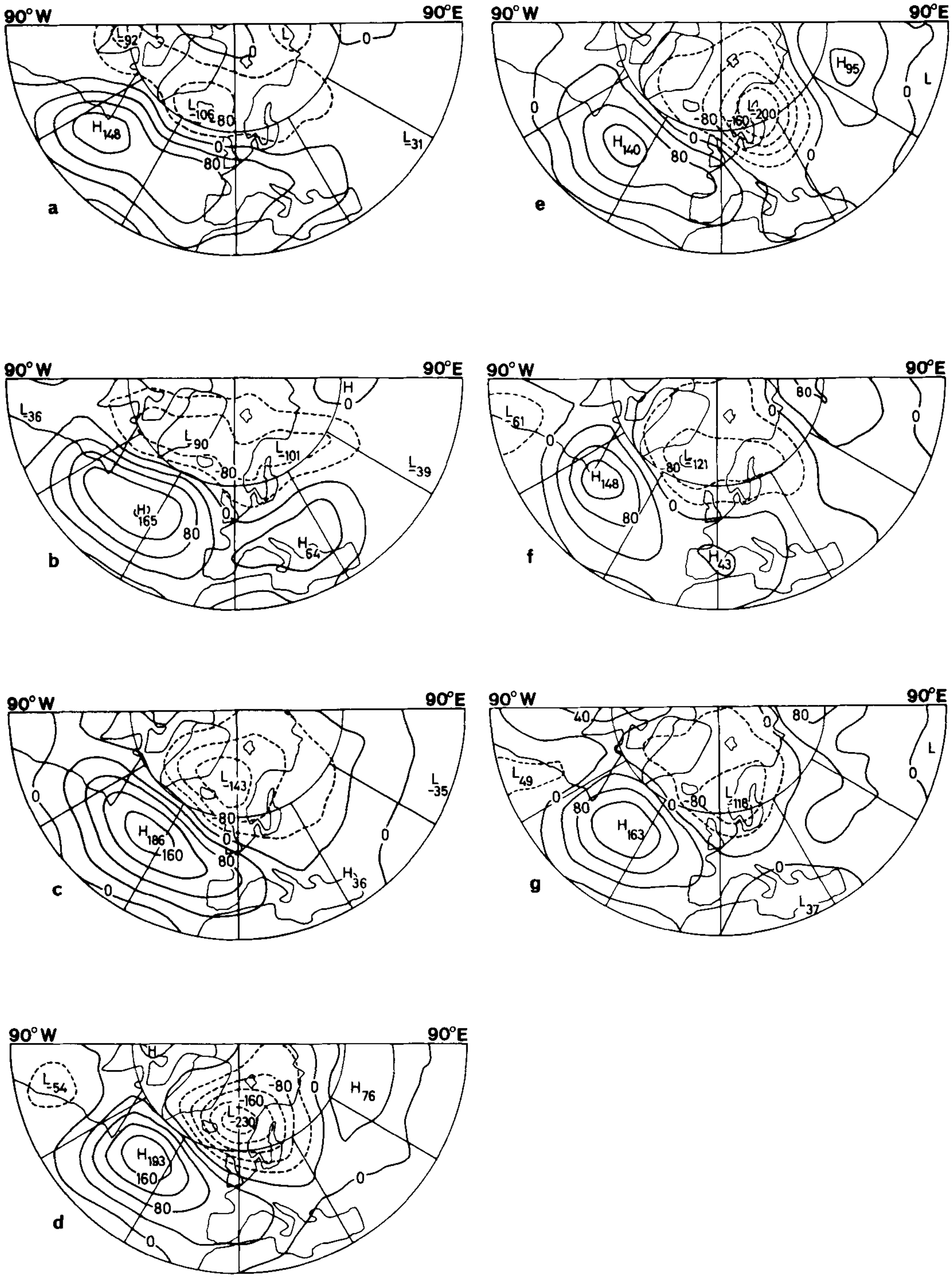

Fig. 6. Evolution of the 500 mb anomaly field (contour interval: 40 gpm) for the western sector; (a) key day − 6, (b) key day − 4, (c) key day − 2, (d) key day, (e) key day + 2, (f) key day + 4, (g) key day + 6. Dashed contours are used for negative values.

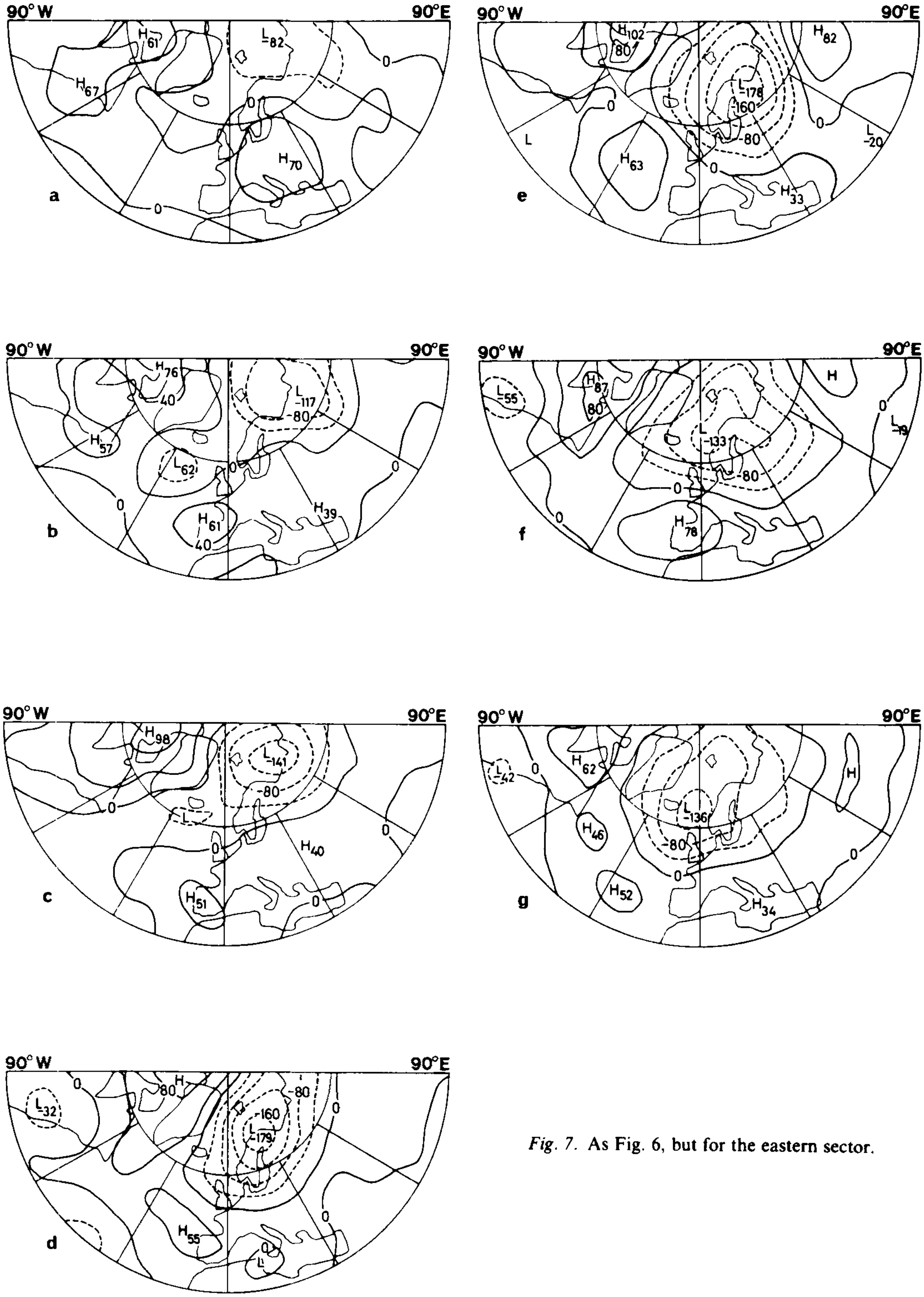

Fig. 7. As Fig. 6, but for the eastern sector.

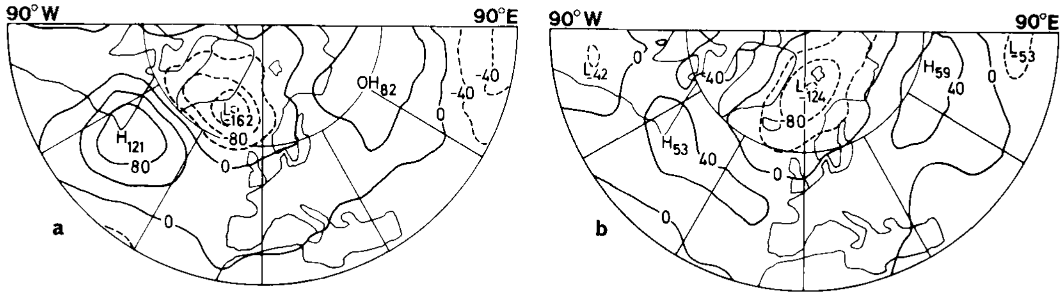

Fig. 8. The anomaly in the 1000–500 mb thickness field (contour interval: 40 gpm). Dashed contours are used for negative values; (a) western sector, (b) eastern sector.

of 1028 mb. The pressure ridge over the Greenland area is stronger than normal for the polar low events in both sectors, 1027 and 1021 mb for the eastern and western sector, respectively.

Figs. 5a, b give the anomaly patterns for the western and eastern sectors, respectively. The essential anomalies in these patterns are the large negative anomaly associated with the 70° N lows and the positive anomaly in the Greenland area. For the western sector, we also find a strong positive anomaly at 50° N and 30° W. This positive anomaly is not found for the eastern sector cases.

3.2. *The synoptic flow pattern at 500 mb*

The 500 mb anomaly patterns for the western and eastern sectors are given in Figs. 6d, 7d, respectively. We find similar anomaly patterns as those at the surface. The values of the anomalies are large compared to Businger's values, especially for the western sector where the negative anomaly close to the Greenwich meridian has a value of −230 gpm. For this sector, we find a positive anomaly of 193 gpm associated with the Azores High. The reason why this anomaly pattern differs so much from the anomaly pattern presented by Businger (1985) may be that we have used winter season cases only and that we have divided the polar low events into two geographically separated groups. Furthermore, the smaller values of the eastern sector anomalies compared to the western sector may be explained by the large scattering of the synoptic scale low pressure centers shown in Fig. 2.

For the 500–1000 mb thickness, the anomalies are given in Fig. 8. From the anomalies for the western sector, we find the northerly air flow to be about 8 °C colder than normal. For the eastern sector, the air is about 6°C colder than normal. This anomalous cold air is situated in the northerly air flow west of the surface low-pressure centre. A westward tilt with height in the negative anomalies will therefore be expected. For the western sector events, we find another marked anomaly. The air in the southerly flow west of the Atlantic High pressure centre is about 6 °C warmer than normal in the 500–1000 mb layer (see Fig. 8a).

The evolution of the anomalies in the composite 500 mb height field for the two sectors is shown in Figs. 6, 7. As seen from these maps, the anomalies persist during a 2-week period. For the eastern sector, the geographical position of the negative anomaly drifts westward early in the sequence (in agreement with Businger's results). For the western sector cases, however, the position of the negative anomaly shows a slight eastward motion in the first part of the sequence. An outstanding feature for the western sector is the strong stationary positive anomaly associated with the Azores High. The anomalies are somewhat larger after than before the key day. This is in agreement with Businger's results, but we find the amplitudes to be more persistent in time.

4. Acknowledgement

Financial support was given by the Norwegian Research Council for Science and the Humanities (NAVF), Nansenfondet and The Norwegian project which is partly financed by oil companies with licences north of 60° N on the Norwegian continental shelf. The authors wish to thank Professors Arnt Eliassen and Ragnar Fjørtoft for valuable discussions.

REFERENCES

Businger, S. 1985. The synoptic climatology of polar low outbreaks. *Tellus 37A*, 419–432.

Carleton, A. M. 1985. Satellite climatological aspects of the "polar low" and "instant occlusion". *Tellus 37A*, 433–450.

Harley, D. G. 1960. Frontal contour analysis of a polar low. *Met. Mag. 89*, 146–147.

Harrold, T. W. and Browning, K. A. 1969. The polar low as a baroclinic disturbance. *Q. J. R. Meteorol. Soc. 95*, 710–723.

Hoem, V., Hoppestad, S. and Rabbe, Å. 1984. Polar low case studies I. Polar lows project, *Technical report No 3*, The Norwegian Meteorological Institute, Oslo, Norway.

Jenne, R. L. 1975. Data sets for meteorological research. *NCAR Tech. Note TN/IA-111*, NCAR, Boulder, CO, USA.

Rabbe, Å. 1975. Arctic instability lows. *Met. Ann. 6*, No. 11.

Stevenson, C. M. 1968. The snowfalls of early December. *Weather 23*, 156–162.

Vinje, T. 1985. Drift composition morphology and distribution of the sea ice field in the Barents Sea. *Skrifter nr. 179C*, Norwegian Polar Research Institute, Oslo, Norway.

Wilhelmsen, K. 1981. The polar low near the Norwegian coast. *Tech. Rep. no. 55*. The Norwegian Meteorological Institute, Oslo, Norway.

Wilhelmsen, K. 1985. Climatological study of gale-producing polar lows near Norway. *Tellus 37A*, 451–459.